Computational Materials Science 206 (2022) 111161

Contents lists available at ScienceDirect

Computational Materials Science

journal homepage: www.elsevier.com/locate/commatsci

Barriers to predictive high-throughput screening for spin-crossover

Daniel Mejía-Rodríguez [a,b,c], Angel Albavera-Mata [a,d], Eric Fonseca [a,d], Dian-Teng Chen [a,b], H-P. Cheng [a,b], Richard G. Hennig [a,d,*], S.B. Trickey [a,b]

[a] Center for Molecular Magnetic Quantum Materials, Quantum Theory Project, University of Florida, Gainesville, FL 32611, United States of America
[b] Department of Physics, University of Florida, Gainesville, FL 32611, United States of America
[c] Environmental Molecular Sciences Laboratory, Pacific Northwest National Laboratory, Richland, WA 99352, United States of America
[d] Department of Materials Science and Engineering, University of Florida, Gainesville, FL 32611, United States of America

ARTICLE INFO

Keywords:
Spin-crossover
Density-functional theory
Transition metal complexes

ABSTRACT

Current spin-crossover (SCO) energy calculations depend on nearly artisanal skill in picking quantum mechanical approximations and computational methods. That is incompatible with automated (work-flow-driven) screening. An acceptable methodology must be quantum mechanically sound, yield both basic structure and property values, and accurate ΔE_{HL} without steering or tuning. Cost vs. accuracy causes focus on density functional theory (DFT). We show by a near-exhaustive study of schemes for calculating the basic molecular high-low spin energy difference, ΔE_{HL}, that presently there is no combination of a constraint-based, non-empirical density functional approximation (DFA) and a set of well-defined semi-empirical corrections to it adequate for such a protocol. Somewhat successful hybrid DFA calculations of ΔE_{HL} are too costly for high-throughput screening of condensed phases. Lower-cost alternatives combine a generalized gradient approximation (GGA) DFA with a Hubbard-U correction (DFT + U). But we show that neither $U = 0$ nor any currently available unsteered U calculation gives a decent ΔE_{HL} value for [Mn(taa)] without also degrading molecular structure or property predictions. Moving to the SCAN meta-GGA does not solve the problem. The revised-restored SCAN (r^2SCAN) meta-GGA together with its deorbitalized version r^2SCAN-L give improved but not wholly satisfactory results. We also document and diagnose several non-obvious technical and procedural sensitivities and inter-code differences. In addition to being a formidable challenge to DFA development, the lack we delineate is a major impediment to progress in the development of quantum materials and spintronics.

1. Introduction

1.1. Context

Spin-crossover (SCO) is the much-studied phenomenon typically observed in transition metal complexes with d^4 to d^7 electronic configurations in which a low-spin (LS) and a high-spin (HS) state of a molecule (one of which is the ground state) are energetically sufficiently close that a small perturbation (such as a temperature change) can cause a switch between those states in the condensed phase [1–13]. Generically, such a SCO free energy shift at temperature T and ambient pressure is $\Delta F_{\mathrm{SCO}} = \Delta E_{\mathrm{HL}} - T\Delta S_{\mathrm{HL}}$, where $\Delta E_{\mathrm{HL}} = E_{\mathrm{HS}} - E_{\mathrm{LS}}$ is the energy difference between the HS and LS molecular states, and ΔS_{HL} the corresponding entropy difference.

This accessible bi-stability is of great interest for its potential technological exploitation in quantum information devices. In particular, SCO molecules are an important archetype of a switchable linker molecule, hence signal transmitter, for molecular magnetic quantum materials. Predictive capacity regarding SCO energetics is an essential prerequisite to mastering the materials physics and chemistry needed to design and fabricate systems with reliable, cost-effective control and interrogation of their quantum states. The foreseeable technological context is the high-throughput screening of complicated condensed phases, e.g., SCO complexes at interfaces.

Such screening requires the tools to calculate the state-to-state energetics of the molecular spin manifolds, the kinetics and thermodynamics of aggregate formation (e.g., solid, deposition on surfaces), and characterize quantitatively any changes (with respect to molecular properties) induced by aggregation. In that context, the *scalability* of the procedures is a key characteristic for two reasons. First is the complexity of the molecules themselves: sizes of several hundred atoms are common. Second, SCO is a collective, condensed-phase phenomenon. Computational approaches affordable for the molecule but unaffordable

* Corresponding author at: Department of Materials Science and Engineering, University of Florida, Gainesville, FL 32611, United States of America.
E-mail addresses: daniel.mejia@pnnl.gov (D. Mejía-Rodríguez), aalbaveramata@ufl.edu (A. Albavera-Mata), rhennig@ufl.edu (R.G. Hennig), trickey@qtp.ufl.edu (S.B. Trickey).

https://doi.org/10.1016/j.commatsci.2021.111161
Received 19 October 2021; Received in revised form 16 December 2021; Accepted 17 December 2021

for routine condensed phase studies, therefore, are irrelevant when the objective is high-throughput screening. *Cost-effectiveness* is related. A two to tenfold increase in computational cost for a moderate increase in accuracy may be worthwhile for investigating a few systems yet be a prohibitive increment for the many thousands or tens of thousands of calculations needed in high-throughput mode.

Reliability enters as well. The methodology must be connected properly to well-understood quantum mechanical methods. *Ad hoc* combinations of independent approximations that work for some poorly understood reason are not, in this context, reliable. The methodology must be predictive, not solely descriptive (*i.e.*, tuned to match some measurements or other calculations). Predictive capacity also requires that there be no consequential methodological differences between the treatments of isolated molecules and the condensed phases. The hands-off treatment of condensed phases *must be consistent with the molecular treatment.*

The methodology also must be *unsteered*. That is, it should not depend upon expert intervention and shaping. Without requiring such involvement, the methodology must provide basic structure and property values of reasonable accuracy as well as ΔE_{HL}. Otherwise, there is no hope of getting the entropic contributions correctly for the right reasons. Here, the distinction between *controllable* and *uncontrollable approximations* is relevant to achieve proper reliability. Integration grids, basis sets, and dispersion interaction approximations are examples of controlled choices for which errors usually can be made arbitrarily small by appropriate selection of computational parameters. In contrast, pseudopotentials, density functional approximations, and many-electron self-interaction corrections are uncontrolled approximations, for which, in general, uncertainties cannot be reduced systematically.

There is extensive literature on SCO with several relevant surveys, including Refs. [1,3,8,9,14]. Broadly, however, the perspective of that vast literature is distinct from the high-throughput screening focus on an even-handed, predictive, reliable, automatable characterization of large numbers of molecules and condensed phases. Computational cost scaling often goes unmentioned or is dismissed, perhaps because relatively small data sets commonly are treated. Consistency between molecular and condensed-phase treatments rarely is considered.

1.2. Issues

In the high-throughput screening context just summarized, even the calculation of ΔE_{HL} for a single SCO molecule poses a severe electronic structure challenge. In particular, the costly scaling with system size of explicit wave-function methods has led to the widespread application of density functional theory (DFT) to the problem. The motivation is that for many systems, modern density functional approximations (DFAs) to the exchange–correlation energy provide an acceptable balance between physical and chemical accuracy and computational cost.

Experience with DFA calculation of SCO energetics, specifically ΔE_{HL}, has been characterized, however, as a trip through a "minefield" [15]. Literature review suggests that even that may seem an understatement. A small but reasonably representative sample of that literature includes Refs. [16–24]. We identify the following issues regarding DFA calculations for SCO molecules:

- ΔE_{HL} magnitudes are small compared to the usual errors of calculations with computationally inexpensive DFAs, not to mention controllable precision issues arising from techniques and their parameters.
- The currently preferred DFAs for molecules are hybrid approximations that combine a generalized gradient approximation (GGA) DFA with a single-determinant exchange, E_x^{D}, contribution with weights typically in the range 10%–15% [7,25–29].
  - The calibration of the weight of the single-determinant exchange in hybrid DFAs often is against experiments. Sometimes results from high-level wave-function calculations are used. Such ab initio calculations have their own spin-manifold difficulties [30]. In addition, there are many versions of the semi-empirical calibration approach.
  - The extra cost (compared to ordinary DFT) of calculating E_x^{D} scales conventionally as $O(N^4)$ with the number of electrons, N, which makes that approach intractable for routine investigation of periodic aggregates of SCO molecules, especially in the high-throughput context.
- A low-cost approximate alternative to inclusion of an E_x^{D} dependence is the DFT + U approach [31]. Determination of U values is mostly empirical, either by fitting or by reliance on expert experience. See, for example, Ref. [32].
- Dispersion corrections to affordable DFAs affect the molecular structures. Depending on the DFA used, some form of van der Waals correction for otherwise omitted dispersion energies often is required [7,20,33–36].
- The prescriptions utilized for SCO energetics often are rather specific to particular magnetic elements. There is, for example, substantial literature about DFAs best suited for Fe complexes [36], but comparatively little information about whether that experience provides guidance for Mn systems.
- Most of the success with DFAs for SCO seems to involve considerable skill in picking convergence and control parameters. Conversely, many failures of various DFAs to predict SCO correctly are documented in, for example, the literature on calibrating hybrid DFA.

For the large-scale prediction of properties of SCO molecular aggregates, this list describes disjointed methodological combinations dependent upon extensive empiricism and expert steering. However useful and valuable that may be for other research, such approaches cannot provide a high-throughput, systematic prediction of SCO in molecules and condensed phases. The question is: Can any of the computationally affordable, constraint-based, non-empirical DFAs be combined with a rational protocol (*i.e.*, a rationally related set of approximations and a well-defined work flow) to provide systematic, cost-effective, accurate prediction of ΔE_{HL} and the basis for eventual calculation of the SCO temperature in aggregates?

Our answer regarding the ΔE_{HL} part is equivocal. For most of the 20 molecules in the database of Ref. [34], the protocol recommended in Ref. [37] succeeds. However, for the complex denoted as [Mn(taa)], that protocol, while doing better than any other simple methodology, is not fully successful. *This is a critically important negative result.* As we also document, getting to that result requires investigating how to control or mitigate a considerable variety of technical and procedural problems that often seem to be ignored in favor of defaults. That is the controllable–uncontrollable error issue.

By detailed analysis of this important negative result for the [Mn(taa)] system, here we provide a stringent perspective on the current computational approaches to a key ingredient of SCO. In particular, we show that there is need (and opportunity) for a new algorithmic route to reliable U values for use with a lower-rung DFA that needs only a small U (below about 1 eV). Less surprisingly, we confirm the importance of van der Waals corrections to lower rung DFAs in order both to handle intramolecular Jahn–Teller structural changes and intermolecular effects in aggregates. And, we show that meticulous analysis of controllable approximations is mandatory for an automated predictive SCO high-throughput workflow with modern DFAs.

The remainder of the paper is structured as follows. Section 2 describes the focus SCO molecule, [Mn(taa)]. Pertinent DFA details are given in Section 3. We survey the codes, technical options, and important grid and numerical convergence sensitivities briefly in Section 4,

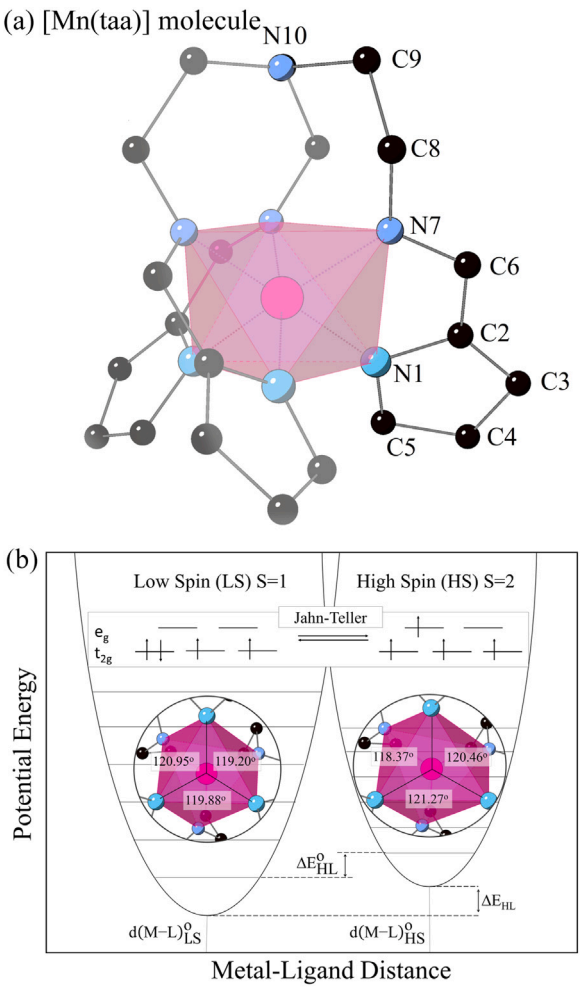

Fig. 1. (a) Structure of the SCO molecule [Mn(taa)] and labels for the symmetry-unique atoms. The octahedron represents the Mn coordination complex. (b) Schematic of the potential energy of the low and high-spin states of [Mn(taa)]. The ground state energy difference is the molecular SCO energy, ΔE_{HL}. The metal-ligand bond lengths elongate in the high-spin state relative to the low-spin state, resulting in a Jahn–Teller distortion and lower vibrational frequencies.

with extensive supporting data in Supplementary Material. Section 5 compares the DFA performance, both for $U = 0$ and $U > 0$, along with a comparative study of some prescriptions for hands-off determination of U. Assessment and implications are presented in Section 6.

2. Focus system

Our focus system is the SCO complex [Mn(taa)]. It is a meridional pseudo-octahedral chelate complex of Mn and the hexadentate tris[(*E*)-1-(2-azolyl)-2-azabut-1-en-4-yl]amine ligand illustrated in Fig. 1(a). Studied originally by Sim and Sinn in 1981 [38], it continues to draw interest as the first known example of a manganese(III), d^4 SCO system. [Aside: The molecule has been studied under several other names, notably [Mn^{III}(taa)] [39–41], [Mn^{III}(TRP)] [38,42], and [Mn^{III}(pyrol)$_3$tren] [43–45]].

Fig. 1(b) illustrates how the SCO energy includes the electronic total energy difference *and* the zero-point energy difference for the two states. An important reality is that the scale for ΔE_{HL}, 1–10 kcal/mol (≈ 40–400 meV), is small compared to the total energies involved [Aside: there are two versions of ΔE_{HL}. Adiabatic is for the two systems at their respective equilibrium geometries, while vertical is for both systems at the same geometry (typically the equilibrium geometry of the lower energy state).]. Pertinent experimental information about [Mn(taa)] symmetry, geometry, and estimated ΔE_{HL} values is compiled in Section I of the Supplementary Material. Also resolved there is an inconsistency in reported bond lengths for the high-temperature, low-spin (HT-LS) phase. The target adiabatic ΔE_{HL} range for this study is 50 ± 20 meV (see Section IB in Supplementary Material); tighter bounds do not seem to be available. That energy is subject to the requirement that the calculation also must provide the correct low-temperature, low-spin (LT-LS) and low-temperature, high-spin (LT-HS) molecular geometries.

[Mn(taa)] has proven to be a more difficult SCO system than others for computation because it combines three intertwined physical challenges. The first is the determination of the ground state. In [Mn(taa)] it is LS, hence $\Delta E_{HL} > 0$. Immediately this is an issue for the use of a simple DFA such as the PBE [46] GGA. Such DFAs suffer from self-interaction error (SIE). [47–52] They tend to favor LS [25,53] because the inadequate exchange magnitude in such DFAs causes inadequate same-spin spatial separation, hence spurious Coulomb repulsion that disfavors the HS state relative to the LS state. One expects, therefore, an overestimated ΔE_{HL}. Such overestimation and the underlying SIE motivate the use of both hybrid DFAs and DFT+U schemes. We discuss this challenge in Section 3.

Second, the [Mn(taa)] complex is large enough to exhibit non-negligible *intramolecular* dispersion interactions. Those have a critical HS-LS difference. Because the HS state involves occupancy of anti-bonding molecular orbitals, the octahedral HS complex tends to have weaker, hence longer, metal-ligand bonds than its LS counterpart. Therefore, the dispersion contribution to the metal-ligand bonds is reduced in the HS case compared to the more compact LS case. This difference in the dispersion contribution to the bonding in the HS and LS complex challenges both simple DFAs and the van der Waals corrections for them [7,20]. The issue is generic to SCO complexes. [Mn(taa)] happens to exemplify it nicely. We discuss the issue of van der Waals corrections in Section 3.3.

Third, the weakening of the metal-ligand bonds for HS relative to LS means a relative softening of vibrational modes. Therefore, the zero-point energy (ZPE) of the HS complex is smaller than for the LS complex. As a consequence, the ZPE provides a stabilizing contribution to the HS state. Notably, the ZPE corrections even to lattice constants have proven to be a non-trivial discriminator among DFAs [54].

This combination of physical and chemical complexities makes [Mn(taa)] a significant test case on which to study the two aspects of the predictive computation of ΔE_{HL} delineated at the outset: the effects of DFA choice (including U determination) and the effects of computational technique, all in the context of being controllable or not.

3. Density functional approximations

The sizable range of ΔE_{HL} values obtained from different DFAs in different codes, see Table 1, motivates the following discussion of the choice of DFAs and corrections.

3.1. Non-empirical lower-rung DFAs

DFA selection clearly is highly influential on results. Many papers on SCO address "optimal" selection. Hence, we cite only a selection that focuses on DFA comparisons and refer to references therein [7,8,10,15,23,34,55–57]. Examination shows much that is incompatible with the requirements for automated, high-throughput screening. There is cafeteria-style combining of separate exchange (E_x) and correlation (E_c) DFAs, along with empirical mixing with E_x^D and even second-order perturbation theory correlation [10,58]. Multiple parameters fitted to large data sets are not uncommon. Most of the DFA optimization seems to have been on Fe SCO complexes.

The cumulative effect of these traits is to limit severely the utility of such heavily semi-empirical DFAs. An expert user may have a clear sense of the chemical space limits within which they are effective.

Table 1
ΔE_{HL} in units of meV for [Mn(taa)] at 0 K calculated from diverse DFAs and a variety of codes. The zero-point effects are omitted.

DFA	Code	ΔE_{HL} (meV)
OPBE[a]	Gaussian	36
B3LYP	NWChem	−69
B3LYP[a]	Gaussian	−10
B3LYP*[a]	Gaussian	157
CAM-B3LYP[a]	Gaussian	−3
HSE06	ORCA	−249
ωB97xD[a]	Gaussian	79
ωB97X-D3(BJ)	ORCA	−283
M06L[a]	Gaussian	−83
SCAN[b]	Q-Chem	350
TPSSh[b]	Q-Chem	185
TPSSh[c]	Gaussian	214
TPSSh[a]	Gaussian	306
TPSSh-D3(BJ)[d]	ORCA	342
M06[a]	Gaussian	−504

[a]Ref. [34]. Mn atom described with def2-QZVP basis, the rest with def2-TZV.
[b]Ref. [24]. Mn atom described with def2-QZVP basis, the rest with def2-TZV.
[c]Ref. [34]. All atoms described with def2-QZVP basis.
[d]Ref. [21]. All atoms described with def2-SVP basis.

But artisanal skills of that sort are valid mainly for interpreting the consequences of carefully selected molecular modifications that are small in a chemically meaningful sense. Those chemical spaces and parametrizations are so constricted and the expert role so large that there is no prospect of such approaches being a general driver of automated high-throughput calculations.

Clarity and motivation for DFA selection can be aided by reasoning from the viewpoint of rigorous DFA development. That is somewhat different from, for example, the seeming pragmatism of Ref. [20]. We restrict attention, therefore, to non-empirical, constraint-based DFAs. (Notice that in DFA development, "non-empirical" is used to mean not fitted to a large data set nor to bonded systems akin to the ones to be studied. Thus there is some parameter determination relative to specific atomic data and "appropriate norms".) This approach provides as much connection as possible with basic quantum mechanics.

Because of their immense popularity, we begin with GGA and GGA + U approaches. There is deep understanding of their behaviors and a vast inventory of materials treated with them. Also appealing is the ubiquitous implementation of GGAs in codes and the fact that GGA calculations are computationally efficient. What we show here, however, is that the intervention of a skilled user is essential. All presently plausible ways of doing intervention-free GGA + U fail for SCO in [Mn(taa)].

The GGA expression for the exchange energy is

$$E_x^{\mathrm{GGA}}[n] = \int d\mathbf{r}\, n(\mathbf{r})\, \varepsilon_x^{\mathrm{unif}}(n)\, F_x(s)\,, \tag{1}$$

where $\varepsilon_x^{\mathrm{unif}}(n)$ is the exchange energy per electron for a homogeneous electron gas of density $n(\mathbf{r})$, the exchange enhancement factor $F_x(s)$ is a function of the dimensionless reduced density gradient $s = |\nabla n(\mathbf{r})| \,/\, \left(2\, k_F\, n(\mathbf{r})\right)$, with $k_F = (3\pi^2 n(\mathbf{r}))^{1/3}$. The corresponding form for the correlation energy $E_c[n]$ need not be recorded here; details depend on the particular GGA.

Despite wide use, GGAs have a limitation that seems inescapable. Their form is too restrictive to enable satisfaction of all the rigorous properties provable for E_x and E_c. Therefore a subset of constraints must be satisfied, with the rest sacrificed. Unsurprisingly, a subset that yields reasonable GGA performance on molecular thermochemistry test sets yields poor performance on crystalline test sets and conversely. An example is PBE [46], the most widely used GGA DFA by far. A shift in parametrization to PBEsol is required to obtain performance on solids [59,60] comparable to PBE for molecules. [Aside: There has been some enthusiasm for using the OPTX [61] semi-empirical E_x^{GGA} DFA [62,63] for Fe SCO complexes. For our purposes, that is problematic on two grounds. In addition to the empiricism, OPTX is wrong for condensed phases with any metallic character because, by construction, it does not have the correct homogeneous electron gas limit.]

Before considering GGA + U, the next rung up the Perdew-Schmidt ladder of DFA complexity [64] is the meta-GGAs. They use an additional functional variable, the Kohn–Sham kinetic energy density, τ, expressed in terms of the KS orbitals $\varphi_i[n]$. Implicitly, a meta-GGA remains a density functional because the orbitals are. Essentially, incorporation of the τ-dependence enables meta-GGAs to switch between a molecule-like GGA and a solid-like GGA depending on the local properties of the density, hence avoiding built-in bias to molecules or solids. This construction allows meta-GGA DFAs to satisfy most of the constraints known from the exact behavior of E_x and E_c.

Until very recently, the most successful meta-GGAs have been SCAN [65,66], TPSS [67], and TM [68]. Recent years have seen interest and hopefulness in the materials physics community about moving to SCAN [65,66] and away from PBE [46] as the *de facto* default DFA. Because SCAN overestimates the magnetization of 3d elemental solids while TPSS and TM do not [69–74], one might suspect that SCAN would favor the HS state of [Mn(taa)] and TPSS the LS state. As noted in Table 1, however, Cirera and Ruiz presented SCAN calculations that gave LS [24] as the [Mn(taa)] ground state by far too much. The underlying issues include the delicate competition of DFA electronic energy differences, contributions from dispersion interactions, geometry change effects, and ZPE contributions (recall above). That competition makes the simple electronic energy difference argument suspect, at least.

Use of SCAN also is hampered by significant numerical instabilities, see Refs. [75,76] and references therein. The newest refinement, r^{2}SCAN [77], adopts but modifies the regularization in Ref. [75] to restore satisfaction of all but one of the constraints satisfied by SCAN, hence the name "revised-restored SCAN" or r^{2}SCAN. In a rapid survey of SCO complexes, two of us found that r^{2}SCAN gives much better molecular ΔE_{HL} values than SCAN [37] on the data set of Ref. [34]. Here we investigate that finding more thoroughly and delineate its implications.

A crucial aspect of DFT in practice that generally is unremarked in the SCO calculation literature is the difference between ordinary and generalized Kohn–Sham (gKS) calculations. It appears first at the meta-GGA rung of the Perdew-Schmidt complexity ladder. The distinction arises from the explicit orbital dependence of the kinetic energy density, $\tau[\varphi]$. It is possible, in principle, to do an ordinary KS calculation (local potential) with a τ-dependent DFA such as r^{2}SCAN or SCAN. That would require solving for the KS potential via the optimized effective potential procedure (OEP) [78,79]. Because OEP calculations add significant computational cost, they are not common. Routine practice instead is gKS calculation with an orbital-dependent exchange–correlation potential. In general, the two are *not* equivalent [80,81]. We are unaware of any study of how SCO predictions from a given orbital-dependent DFA change from gKS to KS (OEP).

The recently developed deorbitalized versions of τ-dependent meta-GGA DFAs provide the opportunity to gain insight into the issue without constructing the OEPs. The deorbitalized meta-GGA DFAs comprise the third DFA class relevant here. Except for Ref. [37], they are unexplored in the SCO context. In a deorbitalized meta-GGA, the τ dependence is replaced by a combination of s and $\nabla^2 n$ dependence [82–84]. Generically, the type is denoted as meta-GGA-L ("L" for Laplacian) DFAs, with their exchange enhancement factors written as $F_x^{\mathrm{mGGA-L}}$. The key point for calculating ΔE_{HL} is this. If the deorbitalization were perfect, the local potential derived from the deorbitalized DFA would be, up to an arbitrary constant, the OEP for the original orbital-dependent DFA. Therefore, results from the local potentials of actual deorbitalized DFAs (which do not replicate their parent DFAs exactly) become useful surrogates for the computationally costly and generally unavailable OEP results.

The deorbitalized SCAN ("SCAN-L") [82,83] does not overestimate the magnetization of the 3*d* elemental solids [74], so the same HS-LS reasoning as for SCAN would suggest that ΔE_{HL} for [Mn(taa)] from SCAN-L might resemble the expected result from a GGA, that is, favor LS. The same expectation arises for TPSS-L, albeit for a different reason; the elemental 3*d* magnetization curves from it are almost the same as for TPSS. Its results match rather closely the PBE magnetization [74]. The deorbitalized version of r^{2}SCAN, called r^{2}SCAN-L, has a somewhat similar relationship; we consider that in detail.

Hybrid DFAs, the fourth class, are both too expensive and too dependent on user tuning to be part of a high-throughput workflow. They are relevant here only for context. To summarize, hybrid DFAs combine an explicitly density-dependent DFA with some fraction of single-determinantal exchange E_x^{D}. Hybrid DFAs almost inexorably have one or more empirical parameters usually set by fitting. The famous, widely used but *ad hoc* B3LYP [85] DFA is an example. One way to understand the effectiveness of hybrid DFAs is that the E_x^{D} contribution offsets enough of the uncontrollable spurious SIE not handled by the explicit DFA to yield a proper HS-LS energetic balance. However, even if the empirical adjustment can be tolerated, handling the explicit E_x^{D} dependence is computationally costly, especially for large periodic systems. That cost issue is ignored almost universally in the chemistry literature.

The cost issue is exacerbated by use of higher rung DFAs such as double hybrids that further incorporate a fraction of MP2 correlation. A recent work [86] that applied 23 DFAs to over two thousand unique transition-metal complexes found that some double hybrids yield ΔE_{HL} values similar to those from lower-rung DFAs, among other properties of interest. That study also showed the high sensitivity of ΔE_{HL} to the choice of DFA, although the most recent r^{2}SCAN and r^{2}SCAN-L meta-GGAs were not included.

3.2. Hubbard U procedures

An alternative to semi-empirical hybrids that is workable in solids is the DFT + U approach [31]. Also semi-empirical, it applies an effective Hubbard model to a localized-state subspace of orbitals to treat their strong on-site Coulomb interaction. The remaining orbitals are treated solely by an ordinary DFA. In the simplified Dudarev et al. scheme [87,88], the energy from a given DFA, E_{DFA}, is modified to become

$$E_{\mathrm{DFT+U}}[n] = E_{\mathrm{DFA}}[n] + \frac{U}{2}\sum_{\sigma} \mathrm{Tr}\left[\hat{n}_{\sigma}(\hat{n}_{\sigma} - 1)\right] . \tag{2}$$

Here $\hat{n}_{\sigma}$ is the number operator for electrons of spin σ in the selected orbital subspace. The U is an effective Coulomb matrix element that is averaged over the subspace states and subsumes both screening and exchange effects.

For our purposes, the challenge is whether the U can be determined in a systematic, algorithmic way that is compatible with high-throughput screening, thus does not require expert intervention. That contrasts with the frequent practice of using U from tabulated values or experience or plausible results obtained by scanning over a U range. Such exploration, even if it could be systematized and automated, would be risky because of the delicate SCO energetic balance between competing states. Furthermore, without expert steering, it is easy for such calculations to become trapped in local minima during electronic and structural optimization.

Three methods for determining U can be dismissed immediately. The first approach employs the constrained DFT method [89], which exploits the DFT ionization potential (IP) theorem [90] and Kohn–Sham eigenvalues from the chosen DFA. However, the SIE and incorrect derivative discontinuity characteristic of lower-rung DFAs impair a Koopmans-like interpretation of the highest Kohn–Sham eigenvalue, with errors for the estimated IP of as much as 2 eV depending on the DFA choice [91] and the Us suffer accordingly. The two other notable means of obtaining U are the DFT+DMFT (dynamical mean-field theory) and DFT+cRPA (constrained random phase approximation) [92] schemes. Typically, such procedures require auxiliary codes, are not readily amenable to automated self-consistent calculations, and implicate substantially higher computational costs. Additionally, there are technical implementation challenges [93,94].

We investigated two related, alternative methods for calculating U that appear adaptable to automated high-throughput procedures. They aim to correct the deviation from the correct linear dependence of the energy upon electron number between integers (cation, neutral, anion) that is intrinsic to lower-rung DFAs [95,96]. Representing this deviation from linearity by an effective Hubbard term that is quadratic in the occupation numbers provides an estimate of the coefficient U.

The first of those schemes is the *linear response* (LR) method of Coccocioni et al. [31,97]. In it, U is estimated by the derivative of the on-site occupations with respect to the local potential. That derivative approximates the deviation from the exact linear behavior of the energy between integer electron numbers. The LR method is computationally fairly efficient. Our experience shows that it requires a DFT structural relaxation and six each bare and interacting LR calculations [98,99] for a total of 13 separate DFT calculations to determine U_{LR}. However, the LR method tends to overestimate U compared to empirically validated values. It also is susceptible to numerical noise and problematic for use with systems in which a non-zero U induces a significant geometry change relative to the $U = 0$ geometry [99].

The second approach, a *self-consistent* DFT + U scheme by Kulik et al. [100], includes the effect of structural relaxations. The method exploits the observation that the output U_{out} in the LR method is approximately a linear function of the input U_{in} over a range of comparable U_{out} and U_{in} values. Since the desired U should correct the DFA at $U_{\mathrm{in}} = 0$, U_{out} is extrapolated to $U_{\mathrm{in}} = 0$ to obtain U_{SCF}. The self-consistent method requires three steps. First, the system is relaxed as a function of U_{in}. Second, U_{out} is calculated for each of the relaxed structures by the LR method. Finally, a linear regime is identified, such that the U_{SCF} obtained by extrapolation to $U_{\mathrm{in}} = 0$ is comparable to the U_{in}. Compared to the LR approach, the self-consistent method increases the computational cost significantly. The extrapolated U_{SCF} captures the nonlinearity for the given DFA in the initial structure. Kulik et al. reported that their scheme modifies the predicted U only slightly, an average of 9% relative to the LR result. They reported, however, that the self-consistent DFT + U procedure is highly susceptible to numerical noise [101].

A potential problem with the self-consistent DFT + U scheme is that the relaxed structure at a given U is not necessarily the lowest energy structure for that U. Getting stuck in local minima and missing the global minimum is a serious issue. A variation of the self-consistent scheme is to iterate, including the geometry relaxation. One starts at a reasonable value of U or at $U = 0$, relaxes the structure, and then calculates U_{LR} from LR. With that U_{LR}, the procedure is repeated until the change in U is judged to be acceptably small. However, even this scheme is still susceptible to numerical noise and local minima in the relaxation and the determination of U [102].

In addition to the local minima in the structural relaxations, DFT+U methods also are susceptible to multiple local minima in the space of electronic configurations, e.g., possible different occupations of the orbitals dominated by localized *d* or *f* symmetry states [103]. Meredig et al. [104] proposed a heuristic U-ramping technique to address this problem. Instead of direct application of a non-zero Hubbard U of plausible magnitude to the problem, one starts at $U = 0$ and increases it in small steps. Ionic relaxations at each new U start with the structure, self-consistent charge density, and Kohn–Sham orbitals obtained from the preceding U value calculation. While this method does not guarantee identification of the lowest-energy minimum at each U value, it does produce a smooth transition to insulating states for metal-oxide systems [104]. To attempt to avoid trapping in non-optimal states, U-ramping can assist in every LR calculation conducted within

the self-consistent DFT+U method. The U-ramping method also can aid in fitting an empirical U value to match the experimental SCO energy. By ramping U for both the LS and HS structures and calculating ΔE_{HL} at each step, an empirical U value can be obtained that agrees with experiments for SCO. That fitting approach is of course not suitable for predictions but can determine the target U to assess automatable U determinations.

Despite the implications of the limitations just discussed for user interventions, we report investigations of these procedures below.

3.3. Van der Waals corrections

A semi-empirical aspect that is unavoidable at present is the handling of van der Waals (vdW) interactions. Despite strong advocacy for the use of controllable dispersion corrections with semi-local DFAs for other significant materials chemistry problems [105–107], their inclusion has not been standard in the SCO literature. See, however, Refs. [20,36] (and references therein) for exceptions. The omission is important because semi-local DFAs (GGA, meta-GGA, meta-GGA-L) do not describe such interactions fully.

The selection of dispersion corrections for use on SCO systems depends on both the DFA and the system. Nevertheless, such corrections generally favor the LS state in complexes of polydentate aromatic ligands by about 4 kcal/mol (≈ 170 meV) [20]. The corrections are most important for those GGAs for which the exchange enhancement factor $F_x(s) \rightarrow \infty$ as $s \rightarrow \infty$ because such DFAs lack any mid-range dispersion contribution. In contrast, there is evidence that the SCAN and r^{2}SCAN meta-GGAs provide a reasonable description of the mid-range dispersion binding. To the limited extent that the issue has been tested, SCAN-L and r^{2}SCAN-L seem to preserve that characteristic of their respective parent meta-GGAs.

The current best practice seems to be to find a vdW correction that is well-adapted to a specific DFA in some rational sense. There are many choices. For SCAN, its authors decided that the rVV10 [108–110] correction was the best choice to retain its non-empirical character. The "r" denotes "revision" with respect to the original VV10 scheme. The revision enables the non-local integral in VV10 to be computed with comparatively good efficiency. However, empirical corrections to SCAN, for example, the DFT-D3(BJ) scheme [111,112], have been shown to yield results comparable with the more involved rVV10 correction [107,113]. We will assume that any vdW correction appropriate for SCAN also is appropriate for SCAN-L, though the assumption has not been tested. We make the same assumption for r^{2}SCAN and r^{2}SCAN-L.

Another important aspect to consider is the use of vdW correction in the structure relaxation versus only for correcting the energy at an equilibrium geometry obtained with an uncorrected DFA. For [Mn(taa)], the latter approach invariably leads to a relative stabilization of the LS state, while the former approach can compensate for that by making the vdW-corrected HS structure comparatively more compact than the uncorrected one. Depending on the magnitude of the vdW correction, such relaxed structures might be unrealistically compact [34].

A significant consideration is the delicacy of the energies involved. The contributions from zero-point energies, dispersion corrections, and relativistic corrections roughly cancel in many 3d metal SCO complexes. Accounting for all three of these effects might yield results similar to those obtained from neglecting all three [34]. Furthermore, the use of small basis sets in atom-centered-basis codes results in non-negligible intramolecular basis set superposition errors. Those tend to provide spurious compensation for the lack of dispersion corrections [106]. Reliance on such error cancellation obviously is not a predictive strategy.

Based on these considerations, we are led to emphasize PBE, SCAN, SCAN-L, r^{2}SCAN, and r^{2}SCAN-L without and with vdW corrections and, correspondingly, without or with Hubbard U augmentation. For context, at various points, we report illustrative results also from optB86-vdW-DF [114], a reparametrized version of the B86 exchange functional used along with the vdW-DF correlation functional [115], revPBE [116], the revised PBE exchange from Zhang and Yang, TPSS [67], TPSSh [117], a TPSS global hybrid in which there is a 10% E_x^{D} contribution, and B3PW91[118], the first global hybrid proposed by Becke.

4. Computational methods

This study used four electronic structure codes: deMon2k [119], Gaussian09 [120], and NWChem [121,122] for isolated molecules and VASP [123] version 5.4.4 for molecules in a periodic environment. To compare the quality of results from various DFAs, it is essential to identify and control against any effects of the computational techniques used. Such effects can arise from differences between all-electron molecular codes and plane-wave, projector-augmented wave (PAW) periodic codes. Technique issues include basis set size or plane-wave cutoff, hardness (compactness) of PAW cores, use of variational Coulomb fitting, choices for correction terms of various kinds, numerical grid densities, convergence criteria, as well as procedural and approximation options available in some codes but not others. Section II in the Supplementary Material provides an extensive discussion of pertinent details on all these matters. Suffice it to say here that some conventional or default practices do not work well for SCO.

Numerical grids are particularly important. Experience has shown that the integration grids used with the SCAN and SCAN-L DFAs must be quite dense. Specifically, the energies and their spatial gradients from those DFAs converge rather slowly with respect to the number of radial shells per atom [76,113], but the convergence of the energy and gradients with respect to the number of angular points (for a given number of radial shells) is fairly similar to that of an ordinary GGA functional [24]. Section III in Supplementary Material gives details of grid sensitivities for ΔE_{HL} results.

Basis set effects also are delineated there both for Gaussian orbital and plane-wave calculations. With Gaussians, it is possible to make a seemingly reasonable choice, then an improvement thereon that leads to a shift in ΔE_{HL} of about 25%. See discussion associated with Table VI in the Supplementary Material. Our analysis that follows is based upon the best-quality calculations unless otherwise noted. Key choices are documented explicitly in the main text.

The convergence of SCF cycles is documented in Section IV of the Supplementary Material. We encountered several peculiarities. One is an algorithmic weakness in deMon2k that we overcame by mixing approaches. We also documented the need for differentiation of numerical weights to get the forces in deMon2k. That is not the default. In VASP 5.4.4 we encountered an SCF cycle hangup that we traced to a bug and fixed. That too is documented in Section IV of the Supplementary Material.

5. Results

5.1. Without Hubbard U

First, we discuss the effects of DFA choice without a Hubbard U. Regarding structures, we discuss only the ones obtained without symmetry enforcement. Section V of the Supplementary Material provides the structural data for the symmetric system (C_3). Again, we caution that it is fairly easy for a calculation to be forced or trapped in the symmetric state by taking the default inputs in some codes. The behavior of the band gaps and the SCO energy, ΔE_{HL}, are considered in this section.

Table 2 summarizes the ΔE_{HL} results. The most obvious finding is that almost all DFAs give values about one order of magnitude too large compared to the experimentally determined range of 50 ± 20 meV. Though recommended recently [24], SCAN does no better in that regard than PBE, whether with or without vdW corrections. The fact that it gives the LS state as favored is simply a consequence

Table 2
Comparison of ΔE_{HL} (meV) at 0 K for different DFAs. Zero-point effects are neglected but expected to favor the HS state by 40–130 meV. The experimental range for ΔE_{HL} is 50 ± 20 meV. See text for discussion of PBE (VASP) and SCAN (VASP) results [i] and [ii].

DFA	Code	ΔE_{HL} (meV)
PBE	VASP	480 [i]
PBE	VASP	458 [ii]
PBE	deMon2k[a]	479
PBE	deMon2k[b]	449
PBE	NWChem	440
PBE	Gaussian	448
revPBE	Gaussian	492
TPSS	VASP	597
TPSS	VASP[c]	477
TPSS	Gaussian	497
revTPSS	Gaussian	482
SCAN	VASP	456 [i]
SCAN	VASP	409 [ii]
SCAN	deMon2k	428
SCAN	NWChem	390
SCAN-rVV10	VASP	469
SCAN-D3(BJ)	NWChem	456
SCAN-D3(BJ)	NWChem[d]	413
SCAN-L	VASP	698
SCAN-L	deMon2k	702
SCAN-L	NWChem	610
SCAN-L	NWChem[a]	715
r^{2}SCAN	VASP	157
r^{2}SCAN	NWChem	134
r^{2}SCAN-L	VASP	446
r^{2}SCAN-L	NWChem	500
optB86-vdW-DF	VASP	924

[a] Using def2-TZVP and GEN-A2*.
[b] Using either def2-TZVP and GEN-A3*, or def2-QZVP and GEN-A2*.
[c] After zero-curvature correction.
[d] After tightening the Cauchy–Schwarz integral screening threshold.

of the argument given in Section 3. Pure DFAs (those without any E_x^D contribution) such as SCAN and SCAN-L tend to favor LS states [16,17,24]. SCAN-L results also are consistent with that argument. Nevertheless, the LS preference has no reliable quantitative relationship to the actual SCO energetics measured by ΔE_{HL}. Crucially, however, marked improvement is seen for the most recent meta-GGA, r^{2}SCAN, and that improvement is maintained across a wide variety of other SCO complexes [37].

The second point to emphasize is that the code-induced spread of results for PBE and SCAN is as large as 40 and 66 meV, respectively. In other words, controllable approximations and associated code options can cause variations among calculations as large as the quantity being sought. VASP is an interesting example. Moving from more-or-less default choices to stricter cutoffs and more refined options increases ΔE_{HL}, i.e., *worsens* an already large disagreement with experiment for PBE and SCAN. That is not, however, the case for TPSS.

Related to that is the apparent anomaly of two ΔE_{HL} values from the same code, VASP, for PBE and for SCAN. In Table 2 those are labeled "[i]" and "[ii]". They illustrate the effects of seemingly small differences in computational technique. Each of the calculations in the sequence that led to the type-[i] result started from a previously optimized geometry. All of the calculations for type-[ii] started from the geometries for the respective experimental crystal structures (HS or LS). Moreover, [i] used the quasi-Newton ionic relaxation algorithm (`IBRION=1`), whereas [ii] used the conjugate gradient scheme (`IBRION=2`). (The reason for that is the better stability of the conjugate gradient scheme for geometries somewhat distant from the minimum, which is the case for starting structures taken from the crystal.) The other difference is that type-[i] used the Mn_pv PAW whereas type-[ii] used the Mn PAW. The resulting differences in ΔE_{HL} are almost entirely traceable to the effects of the pseudo-potentials themselves and not on the associated optimized geometries. Both PAWs gave PBE ΔE_{HL} 458 and 475 meV respectively, while starting from the optimized geometry from the Mn PAW and relaxing to the Mn_pv PAW gives 475 meV. The combined consequence is arrival at slightly different local minima. The same seemingly tiny technical differences are the cause of the two SCAN results in that table. (The corresponding three PAW cases for SCAN are 405, 396, 394 meV respectively.)

Third, the deorbitalization of SCAN into SCAN-L worsens the calculated SCO energy for [Mn(taa)] by more than 200 meV. This outcome is qualitatively different from the situation in the magnetization of 3*d* elemental solids [74]. There, SCAN-L removes the spurious over-magnetization given by SCAN. The mechanism, however, is essentially the same. The over-magnetization from SCAN corresponds to favoring HS states more strongly than SCAN-L. Hence one expects that ΔE_{HL} from SCAN would be smaller than from SCAN-L. The large worsening of ΔE_{HL} from SCAN-L compared to SCAN also is qualitatively different from the behavior exhibited by the TPSS DFA. It does not over-magnetize the 3*d* elemental solids, and it gives ΔE_{HL} values only moderately worse than SCAN. A similar worsening is observed when r^{2}SCAN is deorbitalized into r^{2}SCAN-L.

Despite the worsening in ΔE_{HL} values obtained with r^{2}SCAN-L vs. r^{2}SCAN, the proposed combination strategy [37] for VASP seems to be the best available. The first step is to do a single-point energy PBE calculation with comparatively loose convergence criteria, then use that density as the starting point for an r^{2}SCAN-L ionic relaxation. Finally, use r^{2}SCAN to compute the SCO energy ΔE_{HL} for the r^{2}SCAN-L relaxed structure. (Or, to be cautious, first check the relaxed structure with r^{2}SCAN.) With this strategy, the similarity of r^{2}SCAN and r^{2}SCAN-L, and the speed-up obtained with r^{2}SCAN-L are exploited.

Fourth, the vdW corrections are rendered mostly immaterial to the ΔE_{HL} errors *if* those corrections are included in the ionic position relaxations. Larger vdW correction effects were seen in Ref. [24] because the vdW contributions were not included during the ionic relaxations. In fact, those contributions must be included along the whole potential energy surface to avoid spurious over-stabilization of the LS state. As previously noted, care must be taken to ensure that all geometries are physically sound (i.e., no overly-compact structures are obtained). Informatively, Tables S5a and S5b of the Supplemental Information to Ref. [21] give the $T = 0$ K electronic total energies for the TPSSh hybrid DFA combined with the Grimme D3 empirical vdW corrections [111] from calculations with the ORCA code [124]. The resulting ΔE_{HL} value is remarkably, but perhaps serendipitously, close to the SCAN result.

Fifth, the automatically generated GEN-A2 auxiliary function set of deMon2k is not well suited to approximate the densities obtained with the Karlsruhe def2 basis sets. This can be seen from the relatively large deviations between the ΔE_{HL} values obtained with deMon2k and NWChem for PBE and SCAN-L. The deviation is not a consequence of code differences since larger auxiliary function sets resolve the discrepancy. In confirmation of that diagnosis, we were able to reproduce those deviations by using the GEN-A2 auxiliary set in NWChem (see SCAN-L results in Table 2).

Sixth, the incorrect implementation of spin-polarized meta-GGA calculations in previous releases of VASP can have uncontrollable, non-negligible effects. For instance, Table 2 shows that the TPSS ΔE_{HL} value changed 120 meV once the bug-fix was applied. The corrected value is in good agreement with that obtained from Gaussian09.

Table 2 also shows the effects of the difference between pure Kohn–Sham and generalized-KS treatments of the mean-field eigenvalue problem. SCAN-L and r^{2}SCAN-L fall in the first category, SCAN and r^{2}SCAN in the second. The result is a shift of some one-electron eigenvalues and a change in the HOMO-LUMO gap. Fig. 2 compares the LS and HS eigenvalues from SCAN, SCAN-L, and PBE DFAs for the respective asymmetric molecular states and Table 3 summarizes the HOMO-LUMO gaps for r^{2}SCAN and r^{2}SCAN-L. In particular, the SCAN HOMO-LUMO gap is larger than the SCAN-L gap. Comparatively subtle differences between SCAN and SCAN-L occupied KS orbital energies also show up in ΔE_{HL}.

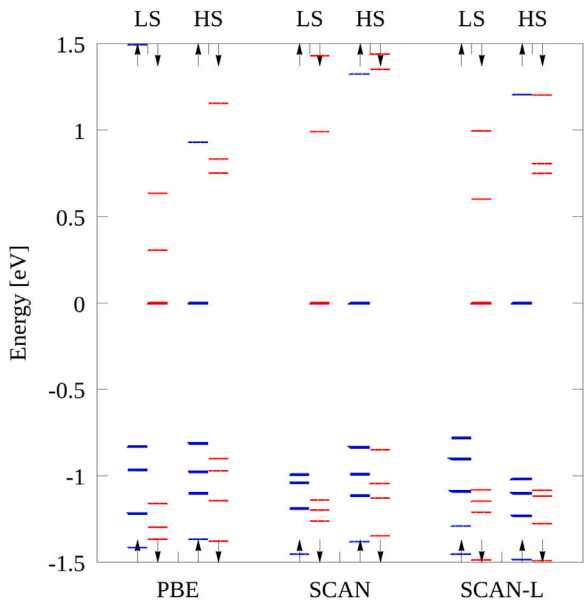

Fig. 2. Discrete eigenvalue spectra for the low- and high-spin configuration calculated with PBE, SCAN and SCAN-L. The blue left line depicts the majority spin and the red right line depicts the minority spin. The *d*-electrons participating in the SCO are depicted with a continuous line. Each spectrum was shifted to $\epsilon_{\text{HOMO}} = 0.0$.

Table 3
HOMO-LUMO gaps in eV for different DFAs obtained from the NWChem and VASP codes.

	DFA	Low-spin		High-spin	
		Majority	Minority	Majority	Minority
NWChem	r^{2}SCAN	2.798	0.832	1.265	2.264
	r^{2}SCAN-L	2.480	0.564	1.107	1.857
	SCAN	2.865	0.956	1.514	2.277
	SCAN-L	2.502	0.583	1.197	1.806
	PBE	2.321	0.315	0.948	1.654
VASP	r^{2}SCAN	2.757	0.756	1.216	2.238
	r^{2}SCAN-L	2.462	0.570	1.088	1.884
	SCAN	2.826	0.869	1.438	2.249
	SCAN-L	2.482	0.565	0.851	1.817
	PBE	2.298	0.261	0.893	1.621

Table 4
Average bond length deviation (Å) with respect to experiment obtained with r^{2}SCAN.

	Low-spin			High-spin		
	Ref.	VASP	NWChem	Ref.	VASP	NWChem
Mn–N(1)	1.975	−0.015	−0.013	2.054	−0.002	+0.005
Mn–N(7)	2.027	−0.012	−0.009	2.121	+0.023	+0.023
Mn–N(10)	3.284	+0.120	+0.095	3.241	+0.153	+0.105
N(1)–C(2)	1.388	−0.002	−0.004	1.385	−0.001	−0.004
N(1)–C(5)	1.351	−0.007	−0.010	1.343	−0.002	0.000
N(7)–C(6)	1.299	+0.012	+0.009	1.295	+0.010	+0.007
N(7)–C(8)	1.469	−0.022	−0.024	1.464	−0.018	−0.020
N(10)–C(9)	1.443	−0.005	−0.007	1.452	−0.011	−0.012

Scrutiny of the underlying molecular structures for these energy differences is needed to assure that those structures are, at least, sensible. The calculated average bond lengths obtained with r^{2}SCAN, and r^{2}SCAN-L and the various codes are shown in Tables 4–5. Corresponding tables for PBE, SCAN, and SCAN-L are in section VI of the Supplementary Material. The predicted C–C and C–H bond lengths, not shown in those Tables, did not vary meaningfully between codes nor DFAs. The reference bond lengths are from Crystallographic Information Files 266992 (LS) and 266995 (HS) respectively.

Table 5
Average bond length deviation (Å) with respect to experiment obtained with r^{2}SCAN-L.

	Low-spin			High-spin		
	Ref.	VASP	NWChem	Ref.	VASP	NWChem
Mn–N(1)	1.975	−0.014	−0.017	2.054	−0.005	−0.002
Mn–N(7)	2.027	−0.014	−0.015	2.121	+0.019	+0.018
Mn–N(10)	3.284	+0.116	+0.085	3.241	+0.148	+0.081
N(1)–C(2)	1.388	+0.003	+0.001	1.385	+0.004	+0.002
N(1)–C(5)	1.351	−0.004	−0.005	1.343	+0.007	+0.004
N(7)–C(6)	1.299	+0.016	+0.015	1.295	+0.014	+0.013
N(7)–C(8)	1.469	−0.017	−0.019	1.464	−0.013	−0.015
N(10)–C(9)	1.443	−0.002	−0.004	1.452	−0.007	−0.008

The PBE geometries turn out to be very similar among the different codes, even for the VASP calculations, for which the PAW pseudopotentials include scalar-relativistic effects. The largest deviation between codes occurs for the Mn–N(10) distance, for which NWChem and Gaussian09 produce a shorter length for both LS and HS configurations than deMon2k and VASP. It is important to note that N(10) is not bonded directly to Mn. Thus, the Mn–N(10) distance might be related to very soft vibrational modes. The enforcement of the displacement criterion in NWChem and Gaussian ionic relaxations can explain the differences seen among the codes for this soft mode reasonably well. A more detailed analysis shows that the ionic relaxation extends one Mn–N(1) bond and shortens the other two in all codes. The same is true for the Mn–N(7) bonds (see Tables X–XII in the Supplementary Material).

The r^{2}SCAN and r^{2}SCAN-L DFAs display a similar uniformity in their structure prediction with the VASP and NWChem codes (see Tables 4 and 5). Generally, the two differ by only about ±0.01 Å. As with PBE, the only notable difference is the Mn–N(10) distance.

In contrast, the SCAN and SCAN-L geometries vary more between codes, indicating their comparatively greater sensitivity to the particular computational setup. For example, the relaxed structures obtained from SCAN with VASP and deMon2k are similar to the PBE results, namely, the elongation of one of the three Mn–N(1) and Mn–N(7) bonds, see Fig. 1(a) for the labels. In contrast, the NWChem relaxation with SCAN led to the elongation of two bonds of each type. However, averaging the three "arms" results in good agreement among different codes, see Table XVI in the Supplementary Material. These differences can be understood readily. [Mn(taa)] has many intramolecular interactions that are subject to the well-known grid and energy cutoff sensitivity of SCAN (and SCAN-L by extension). Those grid sensitivities affect, most prominently, the computed values of the forces acting on the ions. The sensitivities and differences in behavior between a conventional meta-GGA and a deorbitalized counterpart are cautions regarding an automated approach.

For context, Table 6 compares the corresponding deviations of the Mn–N distances with respect to experiment for two sets of DFAs. The first is composed of values in the literature from revPBE, TPSS, revTPSS, B3PW91, and HSE06 along with values for SCAN and TPSSh. None of those DFAs include explicit dispersion interaction corrections. The result is that the Mn–N bonds are too large for the HS configuration. The remaining DFAs with various dispersion corrections constitute the second set. Given the emphasis in quantum chemistry on testing DFAs against thermochemical data, it is perhaps unsurprising that there are no glaring differences.

5.2. With Hubbard *U*

We turn to calculation and use of the Hubbard *U* as a corrective for the poor treatment of the strongly correlated *d*-states near the Fermi level by lower-rung DFAs. That deficiency is the physical origin of the order-of-magnitude discrepancy with respect to experiments in ΔE_{HL} values calculated from all lower-rung DFAs except r^{2}SCAN (recall Table 2). As discussed in Section 3.2, DFT+*U* often is claimed to be a

Table 6
Average bond length deviation [Å] with respect to experiment obtained from several DFAs without dispersion corrections.

	Mn–N(1)	Mn–N(7)	Mn–N(10)
Low-spin			
Exptl.	**1.975**	**2.027**	**3.284**
revPBE	+0.001	0.000	+0.177
SCAN	−0.013	−0.010	+0.106
TPSS	+0.001	−0.002	+0.120
revTPSS	−0.004	−0.008	+0.044
B3PW91	−0.015	−0.002	+0.234
HSE06	+0.001	+0.018	+0.090
TPSSh[b]	−0.008	−0.007	+0.220
vdW-DF-optB86	−0.015	−0.025	+0.123
ωB97X-D3(BJ)	−0.009	+0.015	+0.046
SCAN-rVV10	−0.027	−0.015	+0.128
SCAN-D3(BJ)	−0.018	−0.011	+0.091
TPSSh-D3(BJ)[c]	−0.024	−0.024	+0.032
High-spin			
Exptl.	**2.054**	**2.125**	**3.241**
revPBE	+0.018	+0.040	+0.193
SCAN[a]	+0.002	+0.015	+0.093
TPSS	+0.005	+0.009	+0.137
revTPSS	+0.017	+0.018	+0.042
B3PW91	−0.001	+0.014	+0.288
HSE06	+0.018	+0.034	+0.105
TPSSh[b]	+0.003	+0.012	+0.253
vdW-DF-optB86	−0.011	−0.009	+0.146
ωB97X-D3(BJ)	−0.006	+0.036	+0.067
SCAN-rVV10	−0.023	−0.009	+0.131
SCAN-D3(BJ)	−0.006	+0.014	+0.110
TPSSh-D3(BJ)[a]	−0.004	−0.008	+0.015

[a]Ref. [24]
[b]Ref. [34]
[c]Ref. [21].

Table 7
[Mn(taa)] ΔE_{HL} values for several DFAs with heuristic Hubbard-U correction from MnO. See text regarding second PBE entry.

DFA	U (eV)	ΔE_{HL} (meV)
optB86-vdW-DF	3.90	−158
SCAN+rVV10	3.90	−240
PBE	3.90	−402
PBE	7.13	−711
SCAN	3.90	−358
r^{2}SCAN	3.90	−709
r^{2}SCAN-L	3.90	−329

Table 8
Average bond length deviation (Å) obtained with several DFAs *with* Hubbard-U (eV) corrections.

	U	Mn–N(1)	Mn–N(7)	Mn–N(10)
Low-spin				
Exptl.		**1.975**	**2.027**	**3.284**
optB86-vdW-DF	3.90	+0.004	+0.008	+0.087
SCAN+rVV10	3.90	−0.020	−0.030	+0.094
PBE	3.90	+0.020	+0.029	+0.137
PBE	7.13	+0.071	+0.060	+0.154
SCAN	3.90	+0.005	+0.014	+0.098
r^{2}SCAN	3.90	+0.007	+0.015	+0.100
r^{2}SCAN-L	3.90	+0.011	+0.017	+0.088
High-spin				
Exptl.		**2.054**	**2.125**	**3.241**
optB86-vdW-DF	3.90	+0.012	+0.009	+0.109
SCAN+rVV10	3.90	−0.016	−0.013	+0.106
PBE	3.90	+0.033	+0.036	+0.179
PBE	7.13	+0.053	+0.056	+0.175
SCAN	3.90	−0.003	+0.002	+0.117
r^{2}SCAN	3.90	+0.021	+0.021	+0.129
r^{2}SCAN-L	3.90	+0.018	+0.016	+0.128

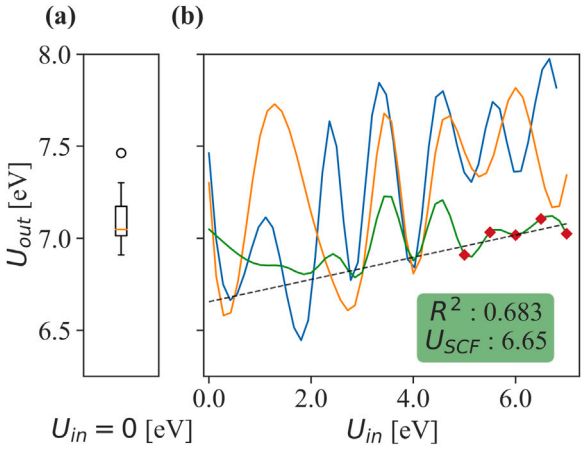

Fig. 3. Calculation of the Hubbard U correction with two different linear response approaches. (a) The box plot shows the distribution of the U_{out} predicted by linear response from eight calculations with $U_{in} = 0$ eV. (b) Illustration of three self-consistent linear response calculations to obtain U_{scf}. Each color denotes a distinct calculation with the PBE DFA on the LS species. Each calculation was initialized with a random wave-function. The dashed line represents the extrapolation to $U = 0$ performed with a linear fit to the calculated values identified with rhombuses.

viable corrective, since increasing U in the context of a simple DFA decreases the calculated ΔE_{HL} [99,125].

An illustrative example of expert use of DFT+U methodology on [Mn(taa)] comes from Yu et al. [32]. They used a microscopic lattice Hamiltonian to study its Jahn–Teller distortion and magneto-electric effects. The on-site term of that Hamiltonian depends directly upon ΔE_{HL} and upon the vibrational frequencies of both the HS and LS states. They determined those quantities with PBE+U calculations in which they tuned the U to be $\approx 3.5 - 4$ eV to be compatible with $\Delta E_{HL} \approx 100$ meV. Then they calculated the vibrational frequencies with the U-corrected functional. They validated the use of the tuned U by doing a constrained RPA calculation of U, which yielded $U = 3.2$ eV.

In essence, their calculation exploited the good, low-cost description of structural properties provided by the PBE DFA and compensated for its SCO deficiencies by a careful tuning and sophisticated validation of U. The problem in our context is that their strategy is wholly incompatible with automated, high-throughput screening.

A common heuristic procedure is to use a U obtained from tabulated values calibrated for similar systems. Such values are available through the Materials Project [126] initiative or via fitting to experimental data using the HOMO-LUMO gap. If table look-up were to be adequate, the U part of the challenge would be overcome. However, the heuristic approach assumes that U does not change significantly between similar systems and is insensitive to structural changes. Expert intervention is required to compensate. To illustrate, Table 7 shows results from combining $U = 3.9$ eV with different DFA choices. That U value was determined from the MnO crystal calibrated using binary formation energies [127]. The result in [Mn(taa)], however, is over-stabilization of the HS state relative to the LS state, i.e., $\Delta E_{HL} < 0$. The heuristic U is too large and increases bond-lengths by 1%–3% relative to base DFA values as shown in Table 8. The addition of van der Waals corrections in optB86-vdW-DF and SCAN+rVV10 reduces the over-stabilization of the HS state, and shortens bond lengths but does not resolve the issue.

The linear response calculation of U with VASP 5.4.4[123] followed published protocols [98,128,129], utilizing the linear dependence of the number of d-electrons in the metal center upon the on-site potential. U is obtained from the diagonal elements of the difference, $\chi_0^{-1} - \chi^{-1}$, between the bare response matrix χ_0 (which does not account for changes in the potential due to charge re-distribution) and the interacting response, χ. [Aside: In VASP 5.4.4, this approach is not available for meta-GGAs, but does work for the deorbitalized meta-GGAs.] Fig. 3(a) shows the range of predicted U values across eight linear response

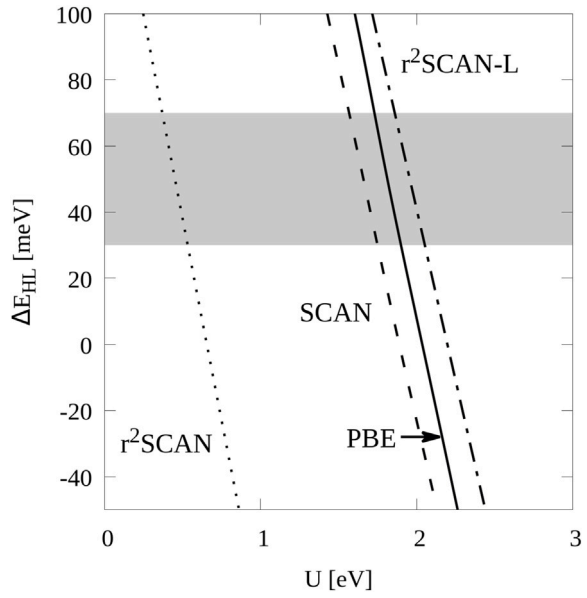

Fig. 4. ΔE_{HL} as a function of U. The shaded area represents the reference target range.

Table 9
ΔE_{HL} values (meV) for several DFAs with a tuned Hubbard-U correction (eV).

DFA	U	ΔE_{HL}
optB86-vdW-DF	3.05	22
SCAN+rVV10	2.79	−150
PBE (LASPH OFF)	1.71	8
PBE	1.82	46
SCAN	1.67	46
r^{2}SCAN	0.45	50
r^{2}SCAN-L	1.96	49

calculations initialized with random wavefunctions by VASP for the LS species. They yield a mean of $\overline{U}_{out} = 7.13$ eV. For r^{2}SCAN-L, a single linear response calculation gave $U_{r^2SCAN-L} = 6.67$ eV. Both magnitudes are significantly larger than the heuristic value from MnO. Thus, both cause a further, unphysical decrease of ΔE_{HL} (relative to the heuristic U result) shown in Table 7 for PBE. Other studies examining Mn^{3+} complexes found similar U values (≈ 7 eV) with this method [130]. Such large values overestimate the splitting of the d-states of the transition metal.

Investigation of the self-consistent protocol described in Section 3.2 showed that it delivers no unambiguously linear region of U_{out} as a function of U_{in} in the interval of values considered in Fig. 3(b). The closest to an approximately linear behavior appears in the interval $5 \leq U_{in} \leq 7$ eV denoted by the rhombuses in that Figure. The extrapolation of $U_{in} \rightarrow 0$ results in $U = 6.65$ eV (with an $R^2 = 0.683$) close to the value calculated with linear response, thus overly large compared to the already oversized heuristic $U = 3.9$ eV. Worse, perhaps, is that no genuine self-consistent U, as defined in this method, was obtainable because of oscillations of U_{out}. The interval of approximate linear behavior $5 \leq U \leq 7$ eV was user-selected. These [Mn(taa)] calculations highlight instances in which the effects of multiple minima and numerical noise severely impede the construction of an automatic, trustworthy Hubbard U determination.

To gain insight into some of these problems, heuristic ramping was used as an analysis tool. The procedure was to tune U for each of four DFAs (PBE, SCAN, r^{2}SCAN, and r^{2}SCAN-L) to yield ΔE_{HL} that matched the estimated target, 50 ± 20 meV (see Section IB of the Supplementary Material). The ramping was in the interval $0 \leq U \leq 7$ eV with increments of 0.2 eV. The process started with a symmetric [Mn(taa)] with the C_3 symmetry axis aligned along the (111) axis, but relaxed

Table 10
Average bond length deviation (Å) obtained with several DFAs *with* tuned Hubbard-U corrections (eV).

	U	Mn–N(1)	Mn–N(7)	Mn–N(10)
Low-spin				
Exptl.		**1.975**	**2.027**	**3.284**
optB86-vdW-DF	3.05	+0.001	+0.004	+0.099
SCAN+rVV10	2.79	−0.002	+0.004	+0.115
PBE	1.82	+0.007	+0.013	+0.147
SCAN	1.67	+0.014	−0.003	+0.113
r^{2}SCAN	0.45	−0.012	−0.010	+0.118
r^{2}SCAN-L	1.96	−0.012	−0.010	+0.103
High-spin				
Exptl.		**2.054**	**2.125**	**3.241**
optB86-vdW-DF	3.05	+0.011	+0.011	+0.135
SCAN+rVV10	2.79	−0.005	−0.005	+0.013
PBE	1.82	+0.025	+0.032	+0.187
SCAN	1.67	−0.006	−0.005	+0.134
r^{2}SCAN	0.45	+0.007	+0.011	+0.153
r^{2}SCAN-L	1.96	+0.011	+0.012	+0.138

ionic positions were not restricted to that point group. The charge densities and KS orbitals from cycle $N-1$ were used to initialize cycle N. Fig. 4 shows that the interval of interest lies between $0 \leq U \leq 3$ eV and illustrates the strong sensitivity of ΔE_{HL} to U, whereas results for PBE and r^{2}SCAN in Table 9 emphasize the overestimation obtained from the previous three methodologies. This effect is most evident for r^{2}SCAN, which has the smallest U among the set. In addition, bond lengths calculated with tuned Us shown in Table 10 differ, in general, by no more than 3.2% with respect to the values from the heuristic reference $U = 3.90$ eV from Table 8. Note, however, that the bond lengths for each DFA + U exhibit their own specific trends.

One other interpretive point emerges. As remarked in Section 3.2, under the assumption that the magnitude of U can be connected directly with SIE, then, at least for [Mn(taa)], r^{2}SCAN, which has the smallest tuned $U = 0.45$ eV, seems to have the smallest such error. Of the DFAs investigated, it is the most competitive, well ahead of SCAN, r^{2}SCAN-L, and PBE. Such smaller U for meta-GGAs was already noticed in an earlier work by Gautam and Carter using SCAN for the evaluation of oxidation energies for a set of transition metal oxides [131]. The plausibility argument for using small U as a quality probe of a DFA is that in principle, the exact exchange–correlation density functional would provide the correct energy ΔE_{HL} (an increment between two ground states) without reliance on a Hubbard-U correction, hence $U = 0$. Therefore, among a set of DFAs, the one needing the smallest non-zero U to reach the correct ΔE_{HL} would be the closest (assuming appropriate conditions of continuity in function space, metrics, etc.) to the exact exchange–correlation functional.

An important controllable technical matter for VASP is the significant effect on the SCO energy of the aspherical corrections of the PAW potentials. For the PBE DFA, Table 9 shows that the optimal U values are $U_{sph} = 1.71$ eV and $U_{asph} = 1.82$ eV without and with the aspherical corrections, respectively. The aspherical corrections shift the energy by an average of 146 meV for the LS structures and 83 meV for the HS structures across all Hubbard U values tested. The discrepancy of the calculated total energy for these structures thereby affects the interpolated Hubbard U.

6. Outcomes and assessment

We have applied constraint-based, non-empirical DFAs in an almost exhaustive way to the problem of the LS-HS energy difference ΔE_{HL} in the molecular complex [Mn(taa)]. That energy difference is critical to its spin-crossover. [Mn(taa)] was chosen precisely because it presents multiple difficult methodological and technical challenges. The defining perspective of the study is reliable results without expert intervention and steering.

The objectives achieved are delineation of the effects of DFA choice, ancillary approximations (U, van der Waals corrections), and computational techniques upon calculated ΔE_{HL}. We have shown that the GGA exchange–correlation functionals (PBE, revPBE, optB86, B3PW91) and most modern meta-GGA functionals (TPSS, revTPSS, M06L, and SCAN) fail to predict even the correct order of magnitude for ΔE_{HL}. That outcome is particularly striking for SCAN, which has been argued to be predictive.

The solitary exception for simple, inexpensive DFAs is the very recent r^{2}SCAN meta-GGA functional. It provides a reasonably accurate ΔE_{HL} in the context of good accuracy for molecular geometries in both HS and LS states. Furthermore, its deorbitalized counterpart r^{2}SCAN-L provides an opportunity for computationally efficient geometry optimization, thereby providing an opportunity for high-throughput studies of SCO materials. Still, there are cautionary notes. The accuracy of the r^{2}SCAN value of ΔE_{HL} is not great. That DFA also suffers from overmagnetization of elemental 3d solids. To a lesser degree, its deorbitalized counterpart, r^{2}SCAN-L, does so as well. To illuminate the extent of the challenge of predictive treatment of such spin manifold energies, we note that both of those DFAs (and many others) also fail to treat Cr_2 molecular dissociation correctly.

We also have shown that r^{2}SCAN requires van der Waals corrections, and even then, the result is not wholly satisfactory. Critically, those corrections can change the molecular geometry and, hence, ΔE_{HL}. The corrections, therefore, must be used in the calculation, not as post-SCF shifts. However, the van der Waals corrections do not alter the overall relative predictive accuracy of the DFAs considered.

We find that none of the relevant approaches to estimate U (heuristic values from similar systems, estimation from various linear response schemes) is reliable. Without prior knowledge of ΔE_{HL}, the Hubbard U correction done without expert intervention fails. We argue that the U values tuned to match the experimental ΔE_{HL} provide a diagnostic of the appropriateness of the DFA, witness the small value associated with r^{2}SCAN. That may be a clue to some new, automatable determination of U.

For the objective of an automated, high-throughput, predictive SCO screening protocol, our outcome is negative. We have demonstrated that at present there is no plausible combination of a constraint-based, non-empirical DFA and a set of well-defined semi-empirical corrections thereto that provide adequate support for such a protocol. That lack also impairs the application of data mining and machine learning techniques to determine ground-state spin states of transition-metal complexes.[132] This outcome constitutes a significant barrier to the large-scale technological application of computational materials physics to the development of quantum materials and spintronics. It also poses a major challenge to constraint-based DFA development.

CRediT authorship contribution statement

Daniel Mejía-Rodríguez: Conceptualization, Methodology, Writing – original draft, Visualization. **Angel Albavera-Mata:** Conceptualization, Methodology, Writing – original draft, Visualization. **Eric Fonseca:** Methodology, Software, Writing – original draft, Visualization. **Dian-Teng Chen:** Methodology. **H-P. Cheng:** Conceptualization, Resources, Funding acquisition. **Richard G. Hennig:** Conceptualization, Methodology, Resources, Writing – review & editing, Supervision, Project administration, Funding acquisition. **S.B. Trickey:** Conceptualization, Methodology, Resources, Writing – review & editing, Supervision, Project administration, Funding acquisition.

Declaration of competing interest

The authors declare that they have no known competing financial interests or personal relationships that could have appeared to influence the work reported in this paper.

Data availability statement

All molecular structures, and the input and output files of the computation that support the findings of this study are available from the corresponding author upon reasonable request.

Acknowledgments

This work was supported as part of the Center for Molecular Magnetic Quantum Materials, an Energy Frontier Research Center funded by the U.S. Department of Energy, Office of Science, Basic Energy Sciences under Award No. DE-SC0019330. We thank Jie-Xiang Yu for discussion of the determination of ΔE_{HL} in Ref. [32].

Appendix A. Supplementary data

Supplementary material related to this article can be found online at https://doi.org/10.1016/j.commatsci.2021.111161.

References

[1] E. Collet, P. Guionneau, C. R. Chim. XX (2018) 1–19.
[2] H. Li, H. Peng, Curr. Opin. Colloid Interface Sci. 35 (2018) 9.
[3] K. Takahashi, Inorganics 6 (2018) 32.
[4] C. Daul, M. Zlatar, M. Gruden-Pavloví, M. Swart, in: M. Swart, M. Costas (Eds.), Spin States In Biochemistry And Inorganic Chemistry: Influence On Structure And Reactivity, John Wiley and Sons, 2016, p. 7.
[5] M. Shatruk, H. Phan, B.A. Chrisostomo, A. Suleimenova, Coord. Chem. Rev. 289–290 (2015) 62.
[6] A.B. Gaspar, M. Seredyuk, Coord. Chem. Rev. 268 (2014) 41.
[7] K.P. Kepp, Coord. Chem. Rev. 257 (2013) 196–209.
[8] L.M. Lawson Daku, Curr. Inorg. Chem. 3 (2013) 242–259.
[9] J. Cirera, F. Paesani, Inorg. Chem. 51 (2012) 8194–8201.
[10] S. Ye, F. Neese, Inorg. Chem. 49 (2010) 772–774.
[11] I. Krivokapic, M. Zerara, M.L. Daku, A. Vargas, C. Enachescu, C. Ambrus, P. Tregenna-Piggott, N. Amstutz, E. Krausz, A. Hauser, Coord. Chem. Rev. 251 (2007) 364–378.
[12] M. Nihei, T. Shiga, Y. Maeda, H. Oshio, Coord. Chem. Rev. 251 (2007) 2606–2621.
[13] H.A. Goodwin, Top. Curr. Chem. 234 (2004) 23–47.
[14] P. Gütlich, A.B. Gaspar, Y. Garcia, Beilstein J. Org. Chem. 9 (2013) 342.
[15] B.J. Houghton, R.J. Deeth, Eur. J. Inorg. Chem. 2014 (2014) 4573.
[16] E.I. Ioannidis, H.J. Kulik, J. Chem. Phys. 143 (2015) 034104.
[17] S.R. Mortensen, K.P. Kepp, J. Phys. Chem. A 119 (2015) 4041–4050.
[18] J. Cirera, E. Ruiz, Inorg. Chem. 55 (2016) 1657–1663.
[19] D.J. Harding, P. Harding, W. Phonsri, Coord. Chem. Rev. 313 (2016) 38–61.
[20] K.P. Kepp, Inorg. Chem. 55 (2016) 2717.
[21] S. Amabilino, R.J. Deeth, Inorg. Chem. 56 (2017) 2602–2613.
[22] M.M. Flores-Leonar, R. Moreno-Esparza, V.M. Ugalde-Saldívar, C. Amador-Bedolla, ChemistrySelect 2 (2017) 4717–4724.
[23] J. Sirirak, D. Sertphon, W. Phonsri, P. Harding, D.J. Harding, Int. J. Quantum Chem. 117 (2017) e25362.
[24] J. Cirera, E. Ruiz, J. Phys. Chem. A 124 (2020) 5053–5058.
[25] M. Reiher, O. Salomon, B.A. Hess, Theor. Chem. Acc. 107 (2001) 48–55.
[26] H. Paulsen, A.X. Trautwein, J. Phys. Chem. Sol. 65 (2004) 793–798.
[27] L.M. Lawson Daku, A. Vargas, A. Hauser, A. Fouqueau, M.E. Casida, Chem. Phys. Chem. 6 (2005) 1393–1410.
[28] M. Radoń, Phys. Chem. Chem. Phys. 16 (2014) 14479–14488.
[29] A. Slimani, X. Yu, A. Muraoka, K. Boukheddaden, K. Yamashita, J. Phys. Chem. A 118 (2014) 9005–9012.
[30] H.F. Schurkus, D.-T. Chen, H.-P. Cheng, G. Chan, J.F. Stanton, J. Chem. Phys. 152 (2020) 234115.
[31] B. Himmetoglu, A. Floris, S. de Gironcoli, M. Cococcioni, Int. J. Quantum Chem. 114 (2014) 14–49.
[32] J.-X. Yu, D.-T. Chen, J. Gu, J. Chen, J. Jiang, L. Zhang, X. Zhang, Y. Yu, V.S. Zapf, H.-P. Cheng, Phys. Rev. Lett. 124 (2020) 227201.
[33] T. Bučko, J. Hafner, S. Lebègue, J.G. Ángyán, Phys. Chem. Chem. Phys. 14 (2012) 5389–5396.
[34] J. Cirera, M. Via Nadal, E. Ruiz, Inorg. Chem. 57 (2018) 14097–14105.
[35] R. Lo, D. Manna, R. Zbořil, D. Nachtillagová, P. Hobza, J. Phys. Chem. C 123 (2019) 23186–23194.
[36] S. Vela, M. Fumanal, J. Cirera, J. Ribas-Arino, Phys. Chem. Chem. Phys. 22 (2020) 4938–4945.
[37] D. Mejía-Rodríguez, S.B. Trickey, J. Phys. Chem. A 124 (2020) 9889.
[38] P.G. Sim, E. Sinn, J. Am. Chem. Soc. 103 (1981) 241–243.

[39] M. Nakano, G. Matsubayashi, T. Matsuo, Phys. Rev. B 66 (2002) 212412.
[40] M. Nakano, G. Matsubayashi, T. Matsuo, Adv. Quantum Chem. 44 (2003) 617.
[41] S. Kimura, Y. Narumi, K. Kindo, M. Nakano, G. Matsubayashi, Phys. Rev. B 72 (2005) 064448.
[42] P. Guionneau, Dalton Trans. 43 (2014) 382–393.
[43] Y. Garcia, O. Kahn, J.-P. Ader, A. Buzdin, Y. Meurdesoif, M. Guillot, Phys. Lett. A 271 (2000) 145–154.
[44] P. Guionneau, M. Marchivie, Y. Garcia, J.A.K. Howard, D. Chasseau, Phys. Rev. B 72 (2005) 214408.
[45] K. Ridier, S. Petit, B. Guillon, G. Chaboussant, D.A. Safin, Y. Garcia, Phys. Rev. B 90 (2014) 104407.
[46] J.P. Perdew, K. Burke, M. Ernzerhof, Phys. Rev. Lett. 77 (1996) 3865.
[47] J.P. Perdew, A. Zunger, Phys. Rev. B 23 (1981) 5048–5079.
[48] O.A. Vydrov, G.E. Scuseria, J.P. Perdew, A. Ruzsinszky, G.I. Csonka, J. Chem. Phys. 124 (2006) 094108.
[49] T. Tsuneda, K. Hirao, J. Chem. Phys. 140 (2014) 18A513.
[50] G. Moynihan, G. Teobaldi, D.D. O'Regan, Phys. Rev. B 94 (2016) 220104(R).
[51] S.J. Clark, T.W. Hollins, K. Refson, N.I. Gidopoulos, J. Phys.: Condens. Matter 29 (2017) 374002.
[52] B. Santral, J.P. Perdew, J. Chem. Phys. 150 (2019) 174106.
[53] A. Droghetti, D. Alfé, S. Sanvito, J. Chem. Phys. 137 (2012) 124303.
[54] P. Hao, Y. Fang, J. Sun, G.I. Csonka, P.H.T. Philipsen, J.P. Perdew, Phys. Rev. B 85 (2012) 014111.
[55] H. Paulsen, L. Duelund, H. Winkler, H. Toftlund, A.X. Trautwein, Inorg. Chem. 40 (2001) 2201–2203.
[56] J. Conradie, A. Ghosh, J. Phys. Chem. B 111 (2007) 12621–12624.
[57] S. Song, M.-C. Kim, E. Sim, A. Benali, O. Heinonen, K. Burke, J. Chem. Theory Comput. 14 (2018) 2304–2311.
[58] S. Grimme, J. Chem. Phys. 124 (2006) 34108.
[59] G. Csonka, O. Vydrov, G. Scuseria, A. Ruzsinszky, J. Perdew, J. Chem. Phys. 126 (2007) 244107.
[60] J.P. Perdew, A. Ruzsinszky, G.I. Csonka, O.A. Vydrov, G. Scuseria, L.A. Constantin, X.L. Zhou, K. Burke, Phys. Rev. Lett. 100 (2008) 136406.
[61] N.C. Handy, A. Cohen, Mol. Phys. 99 (2001) 403–412.
[62] M. Swart, A.R. Groenhof, A.W. Ehlers, K. Lammertsma, J. Phys. Chem. A 108 (2004) 5479.
[63] M. Swart, J. Chem. Theory Comput. 4 (2008) 2057–2066.
[64] J.P. Perdew, K. Schmidt, AIP Conf. Proc. 577 (2001) 1.
[65] J. Sun, A. Ruzsinszky, J.P. Perdew, Phys. Rev. Lett. 115 (2015) 036402.
[66] J. Sun, R.C. Remsing, Y. Zhang, Z. Sun, A. Ruzsinszky, H. Peng, Z. Yang, A. Pau, U. Waghmare, X. Wu, M.L. Klein, J.P. Perdew, Nature Chem. 8 (2016) 831–836.
[67] J. Tao, J.P. Perdew, V.N. Staroverov, G.E. Scuseria, Phys. Rev. Lett. 91 (2003) 146401.
[68] J. Tao, Y. Mo, Phys. Rev. Lett. 117 (2016) 073001.
[69] E.B. Isaacs, C. Wolverton, Phys. Rev. Mat. 2 (2018) 063801.
[70] S. Jana, A. Patra, P. Samal, J. Chem. Phys. 149 (2018) 044120.
[71] A.H. Romero, M.J. Verstraete, Eur. Phys. J. B 91 (2018) 193.
[72] M. Ekholm, D. Gambino, H.J.M. Jönsson, F. Tasnádi, B. Alling, I.A. Abrikosov, Phys. Rev. B 98 (2018) 094413.
[73] Y. Fu, D.J. Singh, Phys. Rev. Lett. 121 (2018) 207201.
[74] D. Mejía-Rodríguez, S.B. Trickey, Phys. Rev. B 100 (2019) 041113(R).
[75] A.P. Bartók, J.R. Yates, J. Chem. Phys. 150 (2019) 161101.
[76] D. Mejía-Rodríguez, S.B. Trickey, J. Chem. Phys. 151 (2019) 207101.
[77] J.W. Furness, A.D. Kaplan, J. Ning, J.P. Perdew, J. Sun, J. Phys. Chem. Lett. 11 (2020) 8208.
[78] T. Grabo, T. Kreibich, E.K.U. Gross, Mol. Eng. 7 (1997) 27–50.
[79] A. Görling, A. Ipatov, A. Götz, A. Hesselmann, Z. Phys. Chem. 224 (2010) 325.
[80] Z.-h. Yang, H. Peng, J. Sun, J.P. Perdew, Phys. Rev. B 93 (2016) 205205.
[81] J. Perdew, W. Yang, K. Burke, Z. Yang, E. Gross, M. Scheffler, G. Scuseria, T. Henderson, I. Zhang, A. Ruzsinszky, H. Peng, J. Sun, E. Trushin, A. Görling, Proc. Nat. Acad. Sci. (USA) 114 (2017) 2801.
[82] D. Mejía-Rodríguez, S.B. Trickey, Phys. Rev. A 96 (2017) 052512.
[83] D. Mejía-Rodríguez, S.B. Trickey, Phys. Rev. B 98 (2018) 115161.
[84] D. Mejía-Rodríguez, S.B. Trickey, Phys. Rev. B 102 (2020) 121109(R).
[85] P.J. Stephens, F.J. Devlin, C.F. Chabalowski, M.J. Frisch, J. Phys. Chem. 98 (1994) 11623.
[86] C. Duan, S. Chen, M.G. Taylor, F. Liu, H.J. Kulik, Chem. Sci. 12 (2021) 13021.
[87] S.L. Dudarev, G.A. Botton, S.Y. Savrasov, C.J. Humphreys, A.P. Sutton, Phys. Rev. B 57 (1998) 1505–1509.
[88] Y. Zhang, J. Chem. Phys. 141 (2014) 214703.
[89] O.K. Andersen, Z. Pawlowska, O. Jepsen, Phys. Rev. B 34 (8) (1986) 5253–5269.
[90] M. Levy, J. Perdew, V. Sahni, Phys. Rev. A 30 (1984) 2745.
[91] P. Politzer, F. Abu-Awwad, Theor. Chem. Acc. 99 (2) (1998) 83–87.
[92] F. Nilsson, F. Aryasetiawan, Computation 6 (1) (2018) 26.
[93] F. Aryasetiawan, K. Karlsson, O. Jepsen, U. Schönberger, Phys. Rev. B 74 (12) (2006) 125206.
[94] M.E. Arroyo-de Dompablo, A. Morales-García, M. Taravillo, J. Chem. Phys. 135 (5) (2011) 054503.
[95] J. Perdew, R. Parr, M. Levy, J. Balduz Jr., Phys. Rev. Lett. 49 (1982) 1691.
[96] E. Engel, R.M. Dreizler, Density Functional Theory -An Advanced Course, Springer-Verlag, Berlin, Heidelberg, 2011.
[97] M. Cococcioni, S. de Gironcoli, Phys. Rev. B 71 (2005) 035105.
[98] E.B. Isaacs, Linear response, 2019, http://grandcentral.apam.columbia.edu:5555/tutorials/dft_procedures/linear_response_u/index.html.
[99] H.J. Kulik, Troubleshooting common problems with DFT+U, 2011, http://hjkgrp.mit.edu/content/troubleshooting-common-problems-dftu.
[100] H.J. Kulik, M. Cococcioni, D.A. Scherlis, N. Marzari, Phys. Rev. Lett. 97 (2006) 103001.
[101] H.J. Kulik, J. Chem. Phys. 142 (March 2015) (2016) 240901.
[102] H.J. Kulik, N. Marzari, J. Chem. Phys. 133 (2010) 114103.
[103] B. Amadon, F. Jollet, M. Torrent, Phys. Rev. B 77 (2008) 155104.
[104] B. Meredig, A. Thompson, H.A. Hansen, C. Wolverton, A. Van De Walle, Phys. Rev. B 82 (19) (2010) 195128.
[105] L. Goerigk, S. Grimme, J. Chem. Theory Comput. 6 (2010) 1.
[106] S. Grimme, A. Hansen, J.G. Brandenburg, C. Bannwarth, Chem. Rev. 116 (2016) 5105–5154.
[107] L. Goerigk, A. Hansen, C. Bauer, S. Ehrlich, A. Najibi, S. Grimme, Phys. Chem. Chem. Phys. 19 (2017) 32184–32215.
[108] H. Peng, Z.-H. Yang, J.P. Perdew, J. Sun, Phys. Rev. X 6 (2016) 041005.
[109] R. Sabatini, T. Gorni, S. de Gironcoli, Phys. Rev. B 87 (2013) 041108(R).
[110] O.A. Vydrov, T.V. Voorhis, J. Chem. Phys. 133 (2010) 244103.
[111] S. Grimme, J. Antony, S. Ehrlich, H. Krieg, J. Chem. Phys. 132 (2010) 154104.
[112] S. Grimme, S. Ehrlich, L. Goerigk, J. Comput. Chem. 32 (2011) 1456–1465.
[113] J.G. Brandenburg, J.E. Bates, J. Sun, J.P. Perdew, Phys. Rev. B 94 (2016) 115144.
[114] J. Klimeš, D.R. Bowler, A. Michaelides, J. Phys.: Condens. Matter 22 (2010) 22201.
[115] M. Dion, H. Rydberg, E. Schröder, D.C. Langreth, B.I. Lundqvist, Phys. Rev. Lett. 92 (2004) 246401.
[116] Y. Zhang, W. Yang, Phys. Rev. Lett. 80 (1998) 890.
[117] V.N. Staroverov, G.E. Scuseria, J. Tao, J.P. Perdew, J. Chem. Phys. 119 (2003) 12129.
[118] A.D. Becke, J. Chem. Phys. 98 (1993) 5652.
[119] A.M. Köster, G. Geudtner, A. Alvarez-Ibarra, P. Calaminici, M.E. Casida, J. Carmona-Espíndola, V.D. Dominguez, R. Flores-Moreno, G.U. Gamboa, A. Goursot, A. Ipatov, T. Heine, A. de la Lande, F. Janetzko, J.M. del Campo, D. Mejía-Rodríguez, J.U. Reveles, J. Vasquez-Perez, A. Vela, B. Zuniga-Gutierrez, D.R. Salahub, deMon2k, Version 6, The DeMon Developers, Cinvestav, Mexico City, 2018.
[120] M.J. Frisch, G.W. T., H.B. Schlegel, G.E. Scuseria, M.A. Robb, J.R. Cheeseman, G. Scalmani, V. Barone, B. Mennucci, G.A. Petersson, H. Nakatsuji, M. Caricato, X. Li, H.P. Hratchian, A.F. Izmaylov, J. Bloino, G. Zheng, Sonnenberg, J.L. Hada, F.D. J., Gaussian 09, revision A. 02, Gaussian, Inc., Wallingford, CT, 1988, 2009.
[121] M. Valiev, E.J. Bylaska, N. Govind, K. Kowalski, T.P. Straatsma, H.J.J.V. Dam, D. Wang, J. Nieplocha, E. Aprà, T.L. Windus, W. de Jong, Comput. Phys. Comm. 181 (2010) 1477.
[122] E. Aprà, E.J. Bylaska, W.A. de Jong, N. Govind, K. Kowalski, T.P. Straatsma, M. Valiev, H.J.J. van Dam, Y. Alexeev, J. Anchell, V. Anisimov, F.W. Aquino, R. Atta-Fynn, J. Autschbach, N.P. Bauman, J.C. Becca, D.E. Bernholdt, K. Bhaskaran-Nair, S. Bogatko, P. Borowski, J. Boschen, J. Brabec, A. Bruner, E. Cauët, Y. Chen, G.N. Chuev, C.J. Cramer, J. Daily, M.J.O. Deegan, T.H. Dunning, M. Dupuis, K.G. Dyall, G.I. Fann, S.A. Fischer, A. Fonari, H. Früchtl, L. Gagliardi, J. Garza, N. Gawande, S. Ghosh, K. Glaesemann, A.W. Götz, J. Hammond, V. Helms, E.D. Hermes, K. Hirao, S. Hirata, M. Jacquelin, L. Jensen, B.G. Johnson, H. Jónsson, R.A. Kendall, M. Klemm, R. Kobayashi, V. Konkov, S. Krishnamoorthy, M. Krishnan, Z. Lin, R.D. Lins, R.J. Littlefield, A.J. Logsdail, K. Lopata, W. Ma, A.V. Marenich, J. del Campo, D. Mejia-Rodriguez, J.E. Moore, J.M. Mullin, T. Nakajima, D.R. Nascimento, J.A. Nichols, P.J. Nichols, J. Nieplocha, A. Otero-de-la Roza, B. Palmer, A. Panyala, T. Pirojsirikul, B. Peng, R. Peverati, J. Pittner, L. Pollack, R.M. Richard, P. Sadayappan, G.C. Schatz, W.A. Shelton, D.W. Silverstein, D.M.A. Smith, T.A. Soares, D. Song, M. Swart, H.L. Taylor, G.S. Thomas, V. Tipparaju, D.G. Truhlar, K. Tsemekhman, T. Van Voorhis, A. Vázquez-Mayagoitia, P. Verma, O. Villa, A. Vishnu, K.D. Vogiatzis, D. Wang, J.H. Weare, M.J. Williamson, T.L. Windus, K. Woliński, A.T. Wong, Q. Wu, C. Yang, Q. Yu, M. Zacharias, Z. Zhang, Y. Zhao, R.J. Harrison, J. Chem. Phys. 152 (18) (2020) 184102.
[123] G. Kresse, J. Furthmüller, Phys. Rev. B 54 (1996) 11169.
[124] F. Neese, WIREs Comput. Mol. Sci. 2 (2012) 73–78.
[125] M. Ohlrich, B.J. Powell, J. Chem. Phys. 153 (10) (2020) 104107.

[126] A. Jain, S.P. Ong, G. Hautier, W. Chen, W.D. Richards, S. Dacek, S. Cholia, D. Gunter, D. Skinner, G. Ceder, K.a. Persson, APL Mater. 1 (1) (2013) 011002.
[127] F. Zhou, M. Cococcioni, C.A. Marianetti, D. Morgan, G. Ceder, Phys. Rev. B 70 (2004) 235121.
[128] H.J. Kulik, Calculating the hubbard U, 2013, http://hjkgrp.mit.edu/content/calculating-hubbard-u.
[129] The VASP manual, 2020, https://www.vasp.at/wiki/index.php/The_VASP_Manual.
[130] J.S. Lim, D. Saldana-Greco, A.M. Rappe, Phys. Rev. B 94 (2016) 165151.
[131] G.S. Gautam, E.A. Carter, Phys. Rev. Mater. 2 (2018) 095401.
[132] M.G. Taylor, T. Yang, S. Lin, A. Nandy, J.P. Janet, C. Duan, H.J. Kulik, J. Phys. Chem. A 124 (2020) 3286.